Gaussian Beam and Physical Optics Iteration Technique for Wideband Beam Waveguide Feed Design

W. Veruttipong, J. C. Chen, and D. A. Bathker
Ground Antennas and Facilities Engineering Section

The Gaussian beam technique has become increasingly popular for wideband beam waveguide (BWG) design. However, it is observed that the Gaussian solution is less accurate for smaller mirrors (approximately $< 30\lambda$ in diameter). Therefore, a high-performance wideband BWG design cannot be achieved by using the Gaussian beam technique alone. This article demonstrates a new design approach by iterating Gaussian beam and BWG parameters simultaneously at various frequencies to obtain a wideband BWG. The result is further improved by comparing it with physical optics results and repeating the iteration.

I. Introduction

Geometrical optics (GO) is a well-known technique used in the design of many beam waveguide (BWG) feed systems. A BWG feed system is composed of one or multiple feedhorns with a series of flat and curved mirrors arranged so that power can be propagated from the horn through the mirrors with minimum losses. Horns and equipment can thus be located in a large, stable enclosure at an accessible location. While GO is useful for designing high-frequency or electrically large mirrors (approximately $> 50\lambda$ in diameter with -20 dB edge taper), some BWGs may be operated at low frequency and have a mirror size of only about 20λ in diameter. Due to diffraction effects, the characteristics of a field propagated between small BWG mirrors (approximately $< 20\lambda$ in diameter) will be substantially different from the GO field. Therefore, the GO design is not suitable for a high-performance wideband BWG antenna with small BWG mirrors. The Gaussian beam technique has become increasingly popular for wideband BWG design. The Gaussian beam mode is an approximate solution of a wave equation describing a beam of radiation that is unguided but effectively confined near an optical axis. The zero-order mode is normally used in the design. A major advantage of the Gaussian technique is the simplicity of the Gaussian formula, which is easy to implement with negligible computer time.

G. Goubau gave the first mathematical expression of Gaussian modes derived from the solution of Maxwell's equations described by a continuous spectrum of cylindrical waves [1]. T. S. Chu developed the Fresnel zone imaging principle of the Gaussian beam to design a pseudo-frequency-independent BWG feed [2]. S. Betsudan, T. Katagi, and S. Urasaki used a similar imaging tech-

nique to design large ground-based BWG antennas [3]. N. J. McEwan and P. F. Goldsmith developed a simple design procedure based on the Gaussian beam theory for illumination of reflector antennas where the reflector is electrically small or in the near-field of a feed [4].

A comparison of scatter fields calculated by zero-order Gaussian and physical optics (PO) solutions indicates that the Gaussian solution is less accurate for smaller mirrors (approximately $< 30\lambda$ in diameter). Therefore, a high-performance wideband BWG design may not be achieved by using the Gaussian beam technique alone. The purpose of this article is to demonstrate a new design approach by iterating Gaussian beam and BWG parameters to obtain a wideband BWG feed. The result is further improved by comparing the Gaussian beam results with the PO results and repeating the iteration. Details will be described next.

II. Design Geometry

The basic goal is to design a BWG feed system with good performance from 2 to 32 GHz by utilizing mirror sizes of 20λ in diameter with edge taper -23 dB at 2.295 GHz (other frequencies may have different edge tapers). It is also required that all feedhorns be placed in a basement room below the azimuth wheel and track. The feed system must provide a simultaneous operation capability and a fast response feed selection system. The geometry of the BWG antenna is shown in Fig. 1, where M_2, M_3, and M_5 are curved mirrors and M_1, M_4, and M_6 are flat plates. If M_6 is a dichroic plate, an additional reflector and horn, beyond M_6, can provide dual frequency simultaneous operation. All the flat plates are assumed to be sufficiently large and are excluded from the design. The BWG in Fig. 1 can be reduced to a horn and three curved mirrors (Fig. 2) with curved mirrors replaced by thin lenses. Let f_i be the focal length and let D_i be the diameter of lens M_i with edge taper $-T_i$ dB (i = 2, 3, and 5). The horn and mirrors are separated by distances L_i (i = 0, 1, 2, 3), with L_H representing the length of the horn. D_H and D_{SUB} are diameters of the horn and the subreflector, respectively. R and D are the wavefront radius of curvature and the -18-dB-beam diameter of the Gaussian beam at the subreflector, respectively. The -18-dB-beam diameter is defined as the diameter at which the field amplitude has fallen 18 dB from its maximum value.

III. Design Procedure

Different frequencies usually have different values of D. The design goal is to have R and D be constant over the design frequency range with acceptable spillover losses at all mirrors and $D = D_{SUB}$. Three frequencies: 2.295 GHz (S-band), 8.45 GHz (X-band), and 32.0 GHz (Ka-band) are used in the design. Curved mirrors are arranged so that the mirror system has a low cross-polarization. For a different design frequency range, the S-, X-, and Ka-bands can be replaced by low, middle, and high frequencies of the band. Input parameters are operating frequencies, D_{SUB}, D_2, D_3, D_5, and maximum allowable spillover loss (or dB edge taper) at each mirror. The relationship between D_H and R_H is known. The rest of the parameters in Fig. 2 are unknown and are to be determined during the iteration process. The desired ranges of some of the input and output parameters need to be established. The initial values to start the iteration can be obtained by the GO design that roughly fits to antenna structures or other requirements.

The design procedure can be described as follows:

Step 1. The radius of curvature R and beam diameter D at the subreflector are calculated starting from the horn and proceeding through mirrors M_5, M_3, and M_2 to the subreflector by using the zero-order Gaussian mode. Details are shown in the Appendix. Let R_s, R_x, and R_{ka} (D_s, D_x, and D_{ka}) be the radii of curvature (-18-dB-beam diameters) at the subreflector calculated at S-, X-, and Ka-bands, respectively. The unknown parameters are iterated so that $R_s = R_x = R_{ka}$ and $D_s = D_x = D_{ka}$. It is quite easy to have $R_x = R_{ka}$ (as well as $D_x = D_{ka}$). However, in many cases (due to structure constraints, size of mirrors, etc.), the iteration cannot converge to the condition $R_s = R_x = R_{ka}$. Instead, R_s is usually greater than R_x and R_{ka}. Therefore, one might have to accept $R_s > R_x = R_{ka}$.

Step 2. The (R_s, R_x, R_{ka}) and (D_s, D_x, D_{ka}) are recalculated by PO, a more accurate technique, with BWG parameters obtained from Step 1. Recall that the Gaussian solution predicts that $R_s = R_x = R_{ka}$ in Step 1, while PO results show that $R_s > R_x > R_{ka}$. The beam diameters from PO calculations are slightly smaller than the Gaussian results at all frequencies (but the trend may not be consistent for other cases). It is noted that the differences of R calculated from PO and Gaussian software are larger at electrically smaller mirrors.

Step 3. In order to offset the discrepancy between Gaussian and PO results, as indicated in Step 2, Step 1 is repeated and the unknown parameters are iterated so that $R_s < R_x < R_{ka}$, which are approximately the same amounts as indicated in Step 2 but in the opposite sense ("larger" in Step 2 results in "smaller" in Step 3). A nu-

merical example will be provided shortly. A similar adjustment procedure is also applied for the beam diameters D_s, D_x, and D_{ka}.

Steps 2 and 3 can be repeated until an acceptable result is achieved. For simplicity, only radii of curvature at X- and Ka-bands are considered as examples here. In Step 1, after millions of iterations, one obtains $R_x = R_{ka} = 476$ in. The calculation in Step 2 by PO software gives $R_x = 488$ in. and $R_{ka} = 478$ in. with $\Delta R_x = 488 - 476 = 12$ in. and $\Delta R_{ka} = 478 - 476 = 2$ in. In Step 3, the goal is to iterate the unknown parameter so that $R_x = 476 - 12 = 464$ in. and $R_{ka} = 476 - 2 = 474$ in. When Step 2 is repeated with parameters recently obtained from Step 3, the results are $R_x = 477$ in. and $R_{ka} = 476$ in. The radius of curvature $R = 476.5$ in. is chosen for a dual-shaped reflector synthesis.

Table 1 shows a numerical comparison between Gaussian and PO techniques of the BWG configuration shown in Fig. 3. If the PO software is not available, one could use data from Table 1, provided that the new BWG configuration closely resembles the one in Fig. 3. It is noted that discrepancies between PO and Gaussian results are larger for electrically smaller diameters. The discrepancies are less sensitive to the distance between mirrors as long as they are in the Fresnel zone. In a design with the minimum mirror diameter $> 50\lambda$, reasonably good performance can be achieved by implementing only Step 1.

IV. Conclusion

The result from this design technique is shown in Fig. 3, with $f_2 = f_3 = 2580$ in. and $f_5 = 220$ in. The mirror diameters are $D_2 = D_3 = 105$ in., $D_5 = 131.5$ in., with their average edge tapers shown in Table 1. It is noted that the design result shown in Fig. 3 is close to the optimum performance. Some small performance sacrifices are made for cost, structure retrofit, maintenance, and accessibility. Also, some S-band performance is sacrificed in order to achieve very good performances at X- and Ka-bands. Spillover loss at each mirror is listed in Table 2. The spillover loss is calculated by integrating a scattered field calculated by the PO software, with the assumption that there is no tube effect. It is observed from Table 2 that energy is more confined well inside the BWG at higher frequencies since the spillover loss is lower at higher frequencies. Higher gain horns are needed for higher frequencies. Aperture diameters of S-, X-, and Ka-band horns are 4.57λ, 10.02λ, and 15.44λ, respectively. One operating mode for this antenna is simultaneous S-/X-band, with the dichroic surface M_6 reflecting S-band and passing X-band. In another operation mode, M_6 is flipped out of the beam path, allowing Ka-band (32.0 GHz; as well as X-band) to propagate to M_7. Given that M_7 is a dichroic surface, simultaneous X-/Ka-band operation is achieved. By simply rotating M_5, extra frequency bands can be used. In 1993, the NASA Deep Space Network (DSN) will begin construction of three 34-m BWG antennas based on this high-performance design concept.

References

[1] G. Goubau and F. Schwering, "On the Guide Propagation of Electromagnetic Wave Beams," *IRE Trans. Antennas Propagat.*, vol. AP-9, no. 5, pp. 248–256, May 1961.

[2] T. S. Chu, "An Imaging Beam Waveguide Feed," *IEEE Trans. Antennas Propagat.*, vol. AP-31, no. 4, pp. 614–619, July 1983.

[3] S. Betsudan, T. Katagi, and S. Urasaki, "Design Method of Four Reflector-Type Beam Waveguide Feeds," *Japanese Electronics and Communications Society Journal*, vol. J67-B, no. 6, pp. 622–629, June 1984.

[4] N. J. McEwan and P. F. Goldsmith, "Gaussian Beam Techniques for Illuminating Reflector Antenna," *IEEE Trans. Antennas Propagat.*, vol. 37, no. 3, pp. 297–304, March 1989.

[5] T. S. Chu, "Geometrical Representation of Gaussian Beam Propagation," *Bell Syst. Tech. Journal*, vol. 45, no. 2, pp. 287–299, February 1966.

Table 1. Radius of curvatures and beamwidths of fields at the subreflector and average edge tapers of M_2, M_3, and M_5, as shown in Fig. 3

Frequency band	R, in.		D, in.		Average edge taper, dB		
	Gaussian	PO	Gaussian	PO	M_2	M_3	M_5
S	462.2	515.0	138.5	137.9	−22	−26	−21
X	464.1	477.0	136.9	134.5	−29	−28	−32
Ka	473.7	476.0	133.7	133.0	−30	−28	−33

Table 2. Spillover loss of each mirror at 2.295, 8.45, and 32.0 GHz

Mirrors	Spillover losses, dB		
	2.295 GHz	8.45 GHz	32.0 GHz
M_1	0.004	0.006	0.006
M_2	0.051	0.015	0.014
M_3	0.018	0.017	0.017
M_4	0.017	0.005	0.004
M_5	0.075	0.005	0.005
M_6	0.025	0.004	–
M_7	–	0.003	0.004
M_8	–	–	0.003
Total	0.190	0.055	0.053

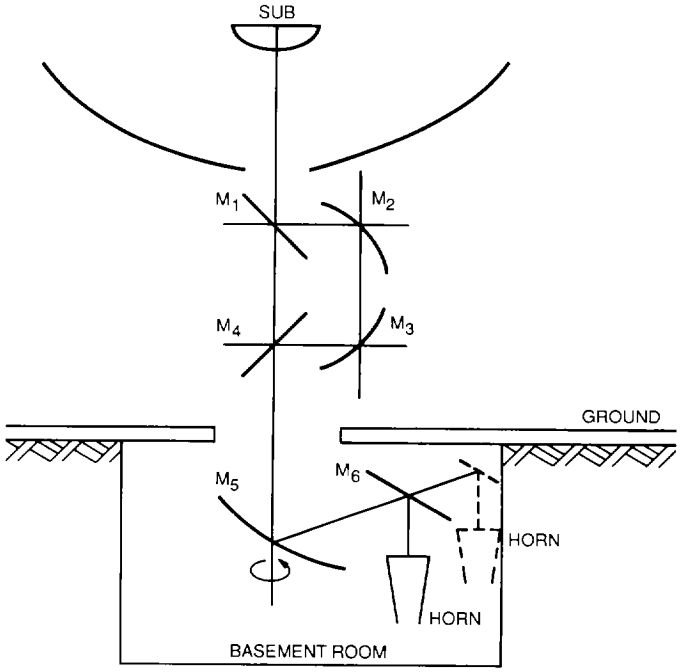

Fig. 1. Beam waveguide design configuration.

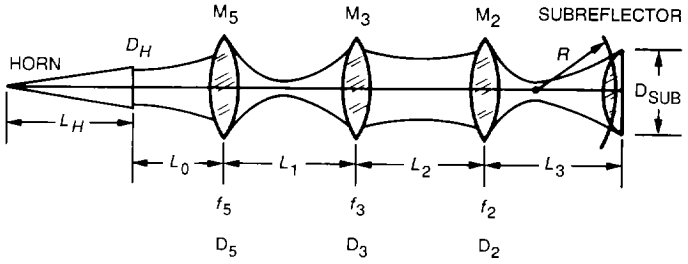

Fig. 2. Beam waveguide design parameters.

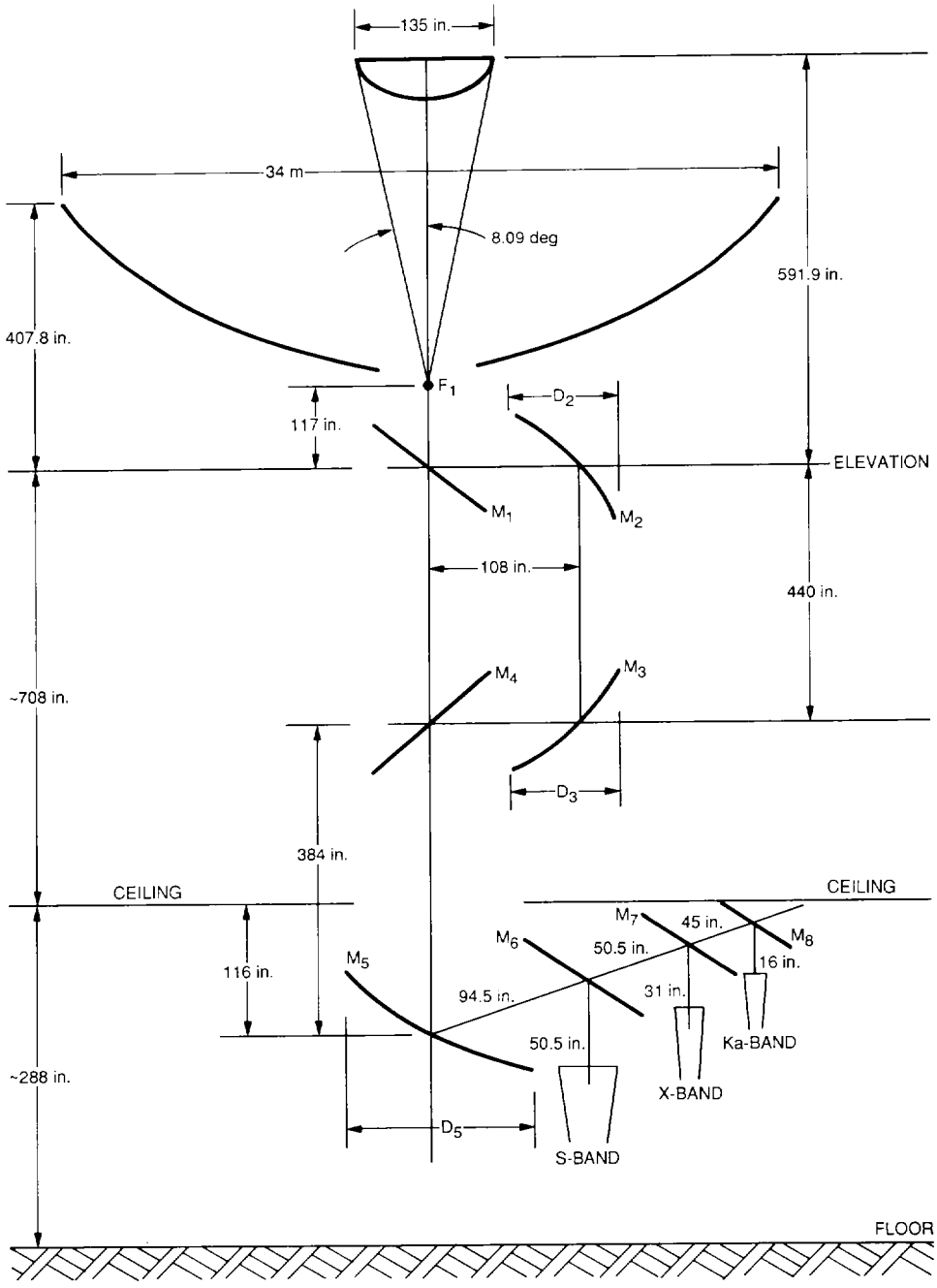

Fig. 3. Detailed dimensions of the beam waveguide configuration.

Appendix

The purpose of this appendix is to show zero-order Gaussian mode expressions used to compute fields from a horn through a series of mirrors and ending at a subreflector.

A. From a Horn to a Mirror (a Thin Lens)

The beam radius and phase front radius of curvature at the aperture of a corrugated horn are

$$\omega_0 = 0.32\ D_H \tag{A-1}$$

and

$$r_0 = \sqrt{L_H^2 + \frac{D_H^2}{4}} \tag{A-2}$$

respectively [2]. The beam radius is defined as the radius at which the field amplitude has fallen 1/e of its maximum values, where D_H and L_H are the diameter and length of the corrugated horn, as shown in Fig. A-1. The radius of curvature on the lefthand side of the thin lens M_1 is [5]:

$$r_1' = \frac{L_0}{\left[1 - \dfrac{1 + L_0/r_0}{\left(1 + L_0/r_0\right)^2 + \left(\lambda L_0/\pi\omega_0^2\right)^2}\right]} \tag{A-3}$$

The beam radius at M_1 (which is the same on both sides of the thin lens) is [5]:

$$\omega_1 = \omega_0\sqrt{\left(1 + L_0/r_0\right)^2 + \left(\lambda L_0/\pi\omega_0^2\right)^2} \tag{A-4}$$

where L_0 is the distance from the horn aperture to the center of the lens (or mirror), and λ is a wavelength of an operating frequency.

The diameter and spillover loss of the lens M_1 with $-T_1$-dB edge taper are each [3]

$$D_1 = 0.6786\ \omega\sqrt{T_1} \tag{A-5}$$

and

$$P_1 = 10\ \log_{10}(1 - e^{-0.2303T_1}) \tag{A-6}$$

Spillover loss in Eq. (A-6) is reasonably accurate for design purposes. After the design is completed, more accurate predictions of the spillover loss will be obtained by direct integration of a scattered field computed by PO and spherical wave expansion software. The radius of curvature on the right-hand side of the lens M_1 can be obtained from a thin lens relation

$$\frac{1}{r_1} = \frac{1}{f_1} - \frac{1}{r_1'} \tag{A-7}$$

where f_1 is the focal length of the lens M_1, and r_1 (as well as r_1') is defined to be positive when its phase front is convex toward the lens surface.

B. Between Mirrors

Similar to Section A, the radius of curvature and beamwidth at the left-hand side of M_2 are

$$r_2' = \frac{L_1}{\left[1 - \dfrac{1 - L_1/r_1}{\left(1 - L_1/r_1\right)^2 + \left(\lambda L_1/\pi\omega_1^2\right)^2}\right]} \tag{A-8}$$

and

$$\omega_2 = \omega_1\sqrt{\left(1 - L_1/r_1\right)^2 + \left(\lambda L_1/\pi\omega_1^2\right)^2} \tag{A-9}$$

where L_1 is the distance between the two lenses. ω_1 and r_1 are given in Eqs. (A-4) and (A-7), respectively. The differences between signs in Eqs. (A-3) and (A-8), and also in Eqs. (A-4) and (A-9) are due to a definition that a radius of curvature of a Gaussian beam is negative when it is concave toward the direction of propagation $(+Z)$, and r_1 is concave toward $+Z$ as in Fig. A-2. The value of r_1 obtained from Eq. (A-7) can be directly substituted into Eqs. (A-8) or (A-9) without changing any of the signs. The diameter and spillover loss of the lens M_2 for $-T_2$-dB taper can be obtained from Eqs. (A-5) and (A-6), with T_1 replaced by T_2. It is noted that M_2 can be a subreflector. The calculations in Section B are repeated for all the rest of the mirrors and the subreflector.

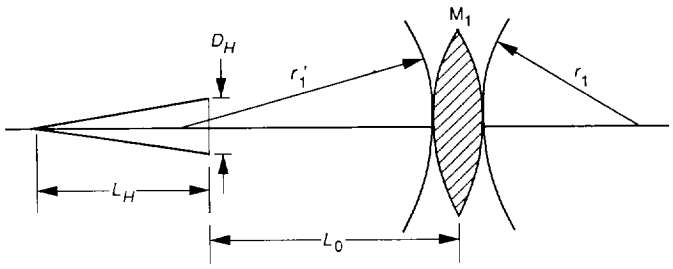

Fig. A-1. The geometry of a circular aperture corrugated horn illuminating a thin lens.

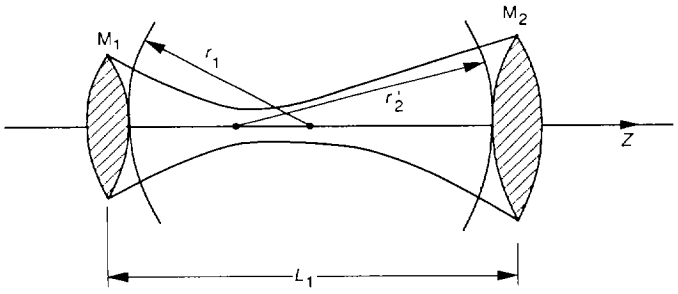

Fig. A-2. The geometry of a Gaussian beam between two lenses.